16TH EUROPEAN CONFERENCE ON EARTHQUAKE ENGINEERING THESSALONIKI 18 - 21 JUNE 2018

COLLAPSE CAPACITY ASSESSMENT OF SKEWED REINFORCED CONCRETE BOX GIRDER BRIDGES RETROFITTED WITH BUCKLING RESTRAINED BRACES

Yuandong WANG[1], Luis IBARRA[2], Chris PANTELIDES[3]

ABSTRACT

This study assesses the seismic performance of a retrofitted three-span reinforced concrete (RC) box girder bridge with asymmetric configuration. The original design of the in-situ California bridge was modified to consider bridge configurations with several skew angles that introduce different asymmetries in the bridge responses, and a retrofit strategy with buckling restrained braces (BRBs). A three-dimensional (3D) model was developed in the software OpenSees, incorporating BRBs between the columns at each bent. These columns were modeled using distributed plasticity to account for material strength and stiffness deterioration. The BRB inelastic behavior was represented using the Menegotto-Pinto model to reproduce its isotropic and kinematic strain hardening properties.

The collapse capacity of bridges with different skew angles before and after being retrofitted with BRBs was evaluated by means of 3D incremental dynamic analysis (IDA) under 21 far-field ground motions, with the consideration of typical experimental failure modes of BRB components. The analysis results indicate that higher skew angles and BRB retrofit have negligible effects on the ultimate collapse capacity of retrofitted bridges after BRB failures. Nevertheless, BRB components can greatly improve the seismic performance of skewed bridges under the design basis earthquake, and the maximum considered earthquake levels. In addition, the implementation of BRB reduces the failure probability since the retrofitted bridges exhibit a better performance under seismic motions, with a larger probability of exceedance, which is represented by integrating fragility curves for different engineering demand parameters (i.e., drift) and the hazard curve for the bridge site.

Keywords: Bridges; Collapse capacity; Three-dimensional; IDA; BRB; Retrofit

1. INTRODUCTION

BRBs implemented in a bridge bent can redistribute and dissipate seismic energy in the transverse direction of the bridge, which reduces potential failure of concrete columns and abutment shear keys (Want et al. 2016). BRBs improve the seismic performance of bridges by decreasing drifts in the bents, as well as steel and concrete strains of the RC columns.

In the IDA method, the structural performance of the evaluated system is assessed by scaling ground motions to multiple levels of intensity, thus producing curves of response parameters versus different intensity levels (Vamvatsikos and Cornell 2002). Even though the common IDA approach is to utilize two-dimensional (2D) models, associated with the hysteretic nonlinear spring models that incorporate strength and stiffness deterioration (Ibarra and Krawinkler 2005) to predict structural collapse performance, few studies have performed IDAs in 3D. For instance, Vamvatsikos and Sigalas (2005) generated a 3D curved bridge model with distributed plasticity fiber elements, and then performed IDAs. In a similar way, Billah and Alam (2014), and He et al. (2016) carried out IDAs to evaluate the seismic performance of retrofitted RC bridges using distributed plasticity models under bidirectional ground

[1]Project Engineer, BHB Consulting Engineers, Salt Lake City, USA, matt.wang@utah.edu
[2]Associate Professor, University of Utah, Salt Lake City, USA, luis.ibarra@utah.edu
[3]Professor, University of Utah, Salt Lake City, USA, c.pantelides@utah.edu

motions. However, a systematic method to define the material properties of distributed plasticity models is still needed to perform 3D IDAs. In addition, the concentrated plasticity and distributed plasticity model have not been previously compared to evaluate their capability to predict structural collapse capacity.

Previous numerical and experimental studies showed that BRB components in the bridge bent help the structure dissipate seismic energy, and improve the seismic performance of bridge in the transverse direction (El-Bahey and Bruneau 2011, Bazaez and Dusicka 2016, Wang et al. 2016, Upadhyay and Pantelides 2017). BRBs have also been proposed to increase the seismic capacity of bridge deck in the longitudinal direction of bridge (Celik and Bruneau 2009, Pantelides et al. 2016). However, few studies have assessed the ultimate capacity of BRBs, especially under seismic events with high magnitude.

In this study, IDA is carried out to investigate the collapse capacity of RC skewed bridges before and after being retrofitted with BRBs. For this purpose, the material properties of distributed plasticity fiber models are calibrated with experimental results that include material deterioration. A 3D distributed plasticity model is first calibrated with a 2D concentrated plasticity model in a 2D realization. The influence of skew angle and BRB retrofit is then studied by using 3D IDAs with the validated distributed plasticity fiber models. The benefit of BRB retrofit is further investigated by comparing the annual frequency of collapse of the original bridges and the retrofitted skewed bridges in the 3D realization.

2. BRIDGE CHARACTERISTICS AND MODELING

2.1 General Description

The evaluated systems are three-span cast-in-place RC box girder skewed bridges. The bridge models are modified based on an existing bridge with a total length of 127.5 m and a 36° skew angle, located in Ripon, CA (Kaviani et al. 2012). The original in-situ bridge is expected to meet the life safety requirements without BRB retrofit, but its operational limits may be exceeded under the design basis earthquake. That is, according to current codes, a seismic retrofit would be needed to keep the bridge's seismic performance under the operational limit states. Then, the retrofit decision depends on the consequences of bridge downtime.

The bridge bent has three circular columns with a diameter of 1.68 m, and a height of 7.38 m. The longitudinal reinforcement in the columns is arranged in bundles of two rebars, with a total of 34 No. 14 rebars (43 mm in diameter). The columns are pin-connected to the foundation and only the interior longitudinal reinforcement is continuously connected to the foundation, with an expansion joint filler injected into the column edges. The piers are supported on 24 H-shaped 305 × 79 steel bearing piles per column, while the seat-type abutments have 9 bearing pads and 40 piles underneath. In this study, the pin connections are utilized at the bent columns, according to Caltrans' recommendations (Caltrans 1999). Several modified bridge models with the same deck length and width are evaluated (Figure 1) with different skew angles (α) with respect to the longitudinal axis.

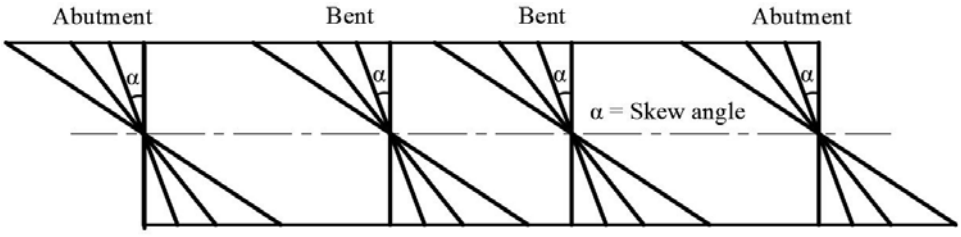

Figure 1. Skew bridge model configurations with different skew angles.

2.2 Bridge Numerical Model

The original numerical model of the investigated bridge was created in OpenSees (McKenna 2010) by Kaviani et al. (2012). Kaviani's model was modified to include BRBs and a new skewed abutment system that was updated from recent experimental tests on soil-structure interaction (SSI) properties of skew abutments (Rollins and Jessee 2012, Marsh 2013), which was applied to a numerical model for the first time. In the longitudinal direction of the bridge abutment, the passive backfill response and the expansion joint are represented with five nonlinear springs and gap elements, respectively (Kaviani et al. 2012). The strength and initial stiffness of the soil springs are defined and modified according to Caltrans' recommendation and recent experimental results (Rollins and Jessee 2012, Marsh 2013). The abutment backfill passive pressure is assumed to be perpendicular to the abutment backwall in bridges with different skew angles. The soil springs are equally spaced and attached to a rigid element, representing the bridge deck. The initial stiffness of the embankment fill material is recommended as 13,333 kN/m/m times the height and length of the abutment backwall under a conservative assumption that the embankment fill material does not meet the requirements of the standard Caltrans specifications (Caltrans 1999).

The soil model considers a reduction of the abutment's ultimate capacity, as the skew angle increases, in accordance with the experimental results from Rollins and Jessee (2012), which results in Equation 1. Furthermore, the properties of the five abutment soil springs are different from each other in the abutment's longitudinal direction. Larger volume of backfill soil is located at the obtuse point behind the abutment stemwall, which results in a larger soil stiffness and strength at the obtuse point than that at the acute point. Due to lack of experimental data, Kaviani et al. (2012) assumed that the largest variation of soil stiffness along the abutment is equal to 30%, when the skew angle $\alpha = 60°$. In this study, however, the spring stiffness variation was re-defined with the largest variation along the skewed abutment as 160% when the skew angle is 60° (Marsh 2013), as shown in Equation 2.

$$R_{skew} = \frac{P_{P-skew}}{P_{P-non\ skew}} = 8.0 \times 10^{-5}\theta^2 - 0.018\theta + 1.0 \quad (1)$$

$$\bar{\beta} = 2.6 \times \frac{\tan \alpha}{\tan 60^0} \quad (2)$$

Using linear-elastic beam-column elements, the deck was modeled with the mass and moment of inertia based on the deck's net area, in agreement with Caltrans requirements. In this study, the bent columns were modeled with concentrated plasticity and distributed plasticity, respectively. In the distributed plasticity model, nonlinear force-based beam-column elements with fiber sections are utilized to capture the material deterioration. Concrete crushing is defined by the Concrete01 material in OpenSees. The compression properties of confined concrete model are the combination of the Modified Kent and Park method (Scott et al. 1982), and the Mander model (Mander 1988). The compression properties of unconfined concrete are defined using Mander's model, as shown in Figure 2.

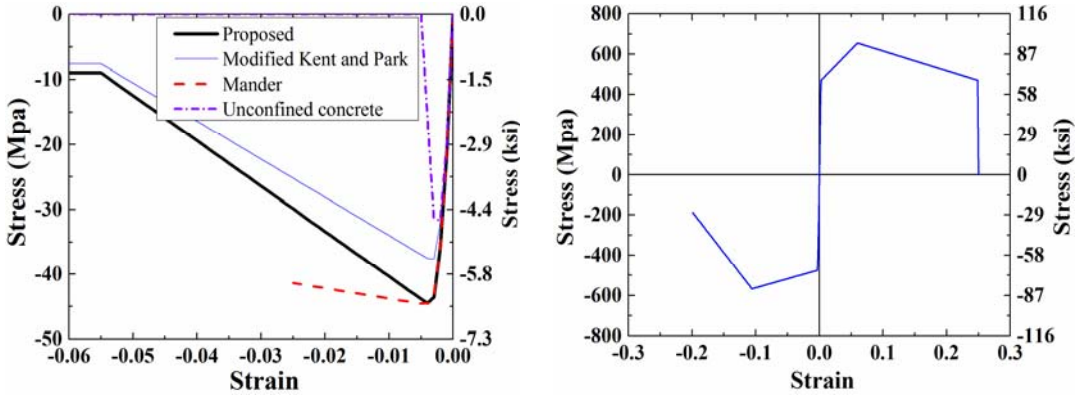

(a) (b)

Figure 2. Stress-strain curves for the distributed plasticity model (a) Concrete, and (b) Steel.

The steel degradation in this study includes softening, buckling after peak strain, and rupture under the large tensile strain. The buckling properties are based on the parameters defined by Dhakal and Maekawa (2002). The softening and rupture of reinforcement is modeled by the hysteretic material in OpenSees (Mckenna 2010) that assumes a reasonable tensile rupture strain of 25%, based on past experimental results (Lowes and Moehle 1995, Mazzoni et al. 1997), as in Figure 2. The main parameters to define the deterioration with distributed plasticity model are shown in Table 1. Shear and torsional stiffness were also included by the section aggregator command in OpenSees. The intermediate stress, strain and maximum buckling strain are defined by Dhakal and Maekawa (2002). In addition, the column segment inserted into the cap beam was assumed to be a rigid link.

Table 1. Parameters for distributed plasticity model.

Confined Concrete	Parameter	Unconfined Concrete	Parameter	Steel	Parameter
Compressive strength	44.9 MPa	Compressive strength	34.5 MPa	Yield Strength	470 MPa
Strain at Max. strength	-0.0028	Strain at Max. strength	-0.0036	Ultimate Strength	655 MPa
Crushing strength	8.3 MPa	Crushing strength	0 MPa	Elastic modulus	2×10^5 MPa
Strain at crushing strength	-0.0550	Strain at crushing strength	-0.0050	Strain hardening ratio	0.01
				Strain at Max. strength	0.060
				Max. tensile strain	0.25
				Intermediate stress	100 MPa
				Intermediate strain	0.106
				Max. buckling strain	0.222

The concentrated plasticity model, on the other hand, captures the nonlinear degradation of members through the deteriorating hysteretic modes proposed by Ibarra and Krawinkler (2005). The deteriorating parameters for the hysteretic model are obtained through the calibration of moment-rotations and hysteretic curves with member experimental tests. The model includes a backbone curve with a negative post-capping stiffness associated with reinforcement buckling and fracture, concrete crushing, and bond failure. Four types of cyclic deterioration can be simulated: basic strength deterioration, post-capping strength deterioration, unloading stiffness deterioration, and accelerated reloading stiffness deterioration. In this study, the empirical parametric equations used to define the RC deterioration model were developed by Haselton and Deierlein (2007), assuming a lognormal distribution for the evaluated parameters. The peak-oriented hysteretic model (Ibarra and Krawinkler 2005, Lignos et al. 2011) is utilized to simulate the columns of the investigated bridge models.

To evaluate the influence of BRB retrofit, BRBs were implemented between every two columns at the bent, and simulated with the Menegotto-Pinto model and the two-node link element in OpenSees, considering both isotropic and kinematic hardening. The connection between the steel gusset plates and the concrete components may require steel rings around the columns (Figure 3), or alternatively, plates attached to the horizontal components at the face of the columns (Bazaez and Dusicka 2016).

2.3 Deterioration Validation

Structural deterioration is vital to perform IDAs, which eventually decides the collapse capacity of investigated structures. Figure 4 presents the comparison of a deteriorating and non-deteriorating bridge

bent with distributed plasticity fiber models under monotonic and quasi-static loading protocol. The two models capture the same elastic stiffness, yield strength, and hardening stiffness, based on the bent's property. However, the deteriorating fiber model can capture the post-capping stiffness that represents the failure of concrete and reinforcing steel, while the non-deteriorating fiber model keeps hardening. This discrepancy proves that the non-deteriorating model leads to non-conservative results during quasi-static or dynamic analysis, since more energy is dissipated by a large hysteretic area. Moreover, the non-deterioration model cannot predict structural instability and collapse, since the strength in the hysteretic loops increases as the drift increases (Figure 4b).

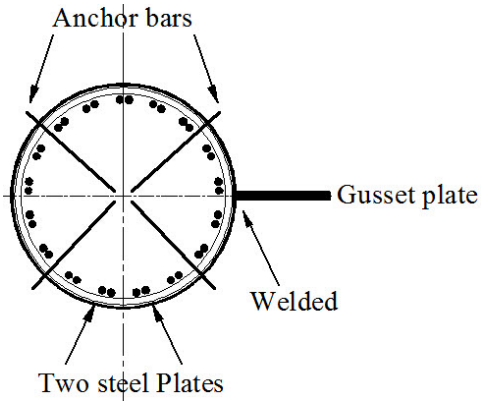

Figure 3. Connection between concrete pier and BRB gusset.

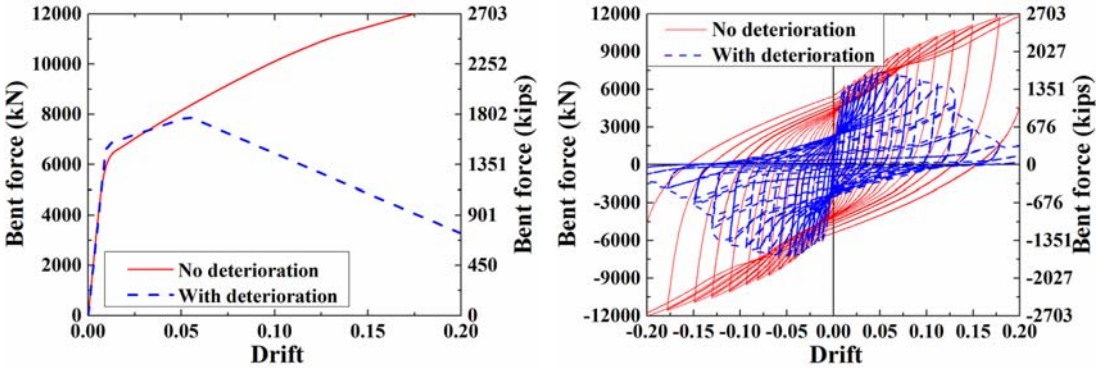

(a) (b)

Figure 4. Distributed plasticity model with and without deterioration (a) Monotonic (b) Cyclic.

3. CONCENTRATED AND DISTRIBUTED PLASTICITY MODEL FOR TWO-DIMENSIONAL INCREMENTAL DYNAMIC ANALYSES (IDAs)

Since the concentrated plasticity model is only applicable in 2D analysis, a straight bridge model is used for comparing resulting IDAs from the concentrated plasticity model and the distributed plasticity model. The numerical analyses included 21 far-field records selected from FEMA P695 (FEMA 2009). For each ground motion set, both horizontal records are first rotated to the principal directions. The major principal direction represents the horizontal record with a larger response acceleration (S_a) at the first period of the bridge in the skew direction. Following an approach similar to that of ASCE 41-06 (ASCE 2007), each set of rotated response spectra was scaled in such a way that the average SRSS response acceleration (S_{a_SRSS}) in the interval $0.2T_{1T} \approx 0.1$ s to $1.5T_{1L} \approx 1.0$ s was equal to 1.3 times the average response acceleration (S_{avg}) of the MCE spectra in this interval (in this case

$S_{a\_SRSS} = 1.3S_{avg} = 0.933$ g). Time history analyses are then performed for the straight bridge ($\alpha = 0°$) under different ground motions and intensity levels. Only one horizontal ground motion is applied along the bridge's transverse direction to keep the analysis in one plane, and thus be able to apply the concentrated plasticity model. Structural global P-Δ effects are considered in these analyses by applying P-Δ coordinate transformations of each bridge column. Note that element P-δ effects are neglected.

In the IDA curves of Figure 5, 21 far-field earthquake records were applied at different seismic levels by scaling S_{a_SRSS} from 0 g to 16 g with an interval of 0.2 g. Individual IDA curves, as well as median, 16th and 84th percentile curves, were generated for the concentrated plasticity (Figure 5a) and the distributed plasticity (Figure 5b); considering second-order P-Δ effects. The statistical curves predict the median collapse capacities with a difference less than 5% for both models, and the structural collapse can be attributed to a large decrease of the bent column's structural resistance. Also in Figure 5, the investigated bridge model does not collapse only under one set of ground motion, which is predicted by both models. The close seismic performance from the IDAs is evidence of the well-defined material degradation from concrete crushing, buckling and tensile fracture of reinforcement.

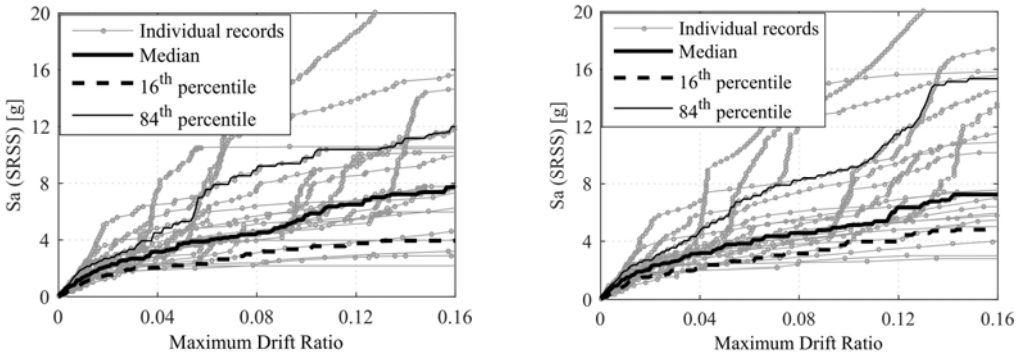

(a) (b)

Figure 5. Sa/g - θmax relationships for the straight bridge models with P-Δ
(a) Concentrated plasticity and (b) Distributed plasticity.

4. **BRB FAILURE DEFINITION FOR INCREMENTAL DYNAMIC ANALYSES (IDAs)**

To generate IDAs, the failure drift of BRB components was derived from two estimators. First, the BRB failure drift was assumed to occur at the maximum axial strain the BRB core plate is expected to reach. An inspection of previous experiments shows that the maximum BRB axial strain rarely exceeds 3.5%, which generally equals to the air gap to BRB core yielding length ratio with a manufactured air gap limit of 75-100 mm (Andrews et al. 2009, Xu and Pantelides 2017). The air gap length is an important indication of BRB failure, since typical failures may occur after the BRB reached this limit in the experiments, such as gusset plate buckling, steel casing bulging, and high-mode buckling of the core. In this study, the BRB axial strain limit is defined as 3.5%, which corresponds to a reasonable upper bound approximation based on statistical results.

The second method correlates BRB axial strain to cumulative failure, based on the recommendations from Andrews et al. (2009). They developed an empirical approach to compute the BRB total cumulative plastic ductility (CPD) capacity, using a database of 76 BRB specimens, of which 34 failed via tensile fracture. Andrews et al. (2009) applied the maximum likelihood estimation method, and consider a damage index based on deformation and dissipated energy, to propose BRB total CPD capacity, which is a function of the BRB core cross-section area, A_C; the BRB core length, L_C; as well as the statistical maximum BRB core area and core length from the 76 cyclic experimental specimens, $(A_C)_{max}$ and $(L_C)_{max}$, respectively. The CPD also depends on the BRB core yield and ultimate strength, f_y and f_u, respectively; and the BRB core yield strain; ε_{yc}.

$$TC = 2^{-21.20} \cdot \left(\frac{A_C}{(A_C)_{max}}\right)^{0.425} \cdot \left(\frac{L_C}{(L_C)_{max}}\right)^{0.044} \times \varepsilon_{yc}^{-3.45} \cdot \left(\frac{f_u}{f_y}\right)^{-1.46} \quad (3)$$

The BRB axial failure strain was then derived for the evaluated bridge, using this CPD criterion. For this purpose, IDAs were carried out on the evaluated bridge model using the 21 far-field records. Figure 6 shows the axial strains reached by the BRB when the total CPD capacity is reached. Note that individual BRB axial strains from Andrews et al. (2009) may reach values higher than 5%, but the median axial strain from the 21 records is 3.1%, which is close to the proposed air gap ratio of 3.5%. Figure 6 also shows that spectral accelerations when the total capacity is reached, are larger than 3 g.

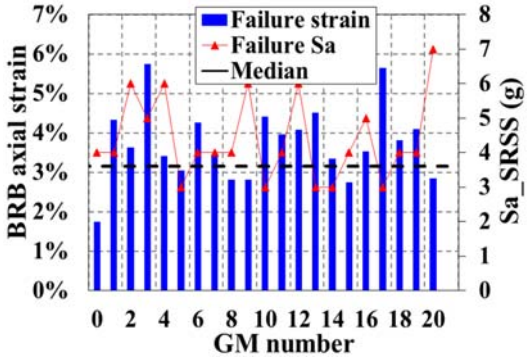

Figure 6. BRB failure under cumulative plasticity ductility method from Andrews et al (2009).

Figure 7 shows the pushover curves for an original three-column RC bent, a combination of two diagonal BRB components, and a BRB retrofitted three-column bent with one BRB component between every column. As observed, BRBs fail once the 3.5% axial strain limit is reached, which is equivalent to a lateral drift of 3.8%. After the BRBs fail, it is assumed that the original RC bent must withstand all the seismic impact, which is reflected by the superposition of the original bent curve and the BRB retrofit bent curve. As structural fuses, BRBs are designed to have a smaller yield displacement than that of the bare bridge bent (El-Bahey and Bruneau 2011, Wang et al. 2016). As a result, the elastic stiffness of BRB components is larger than that of the bare RC bent (Figure 7).

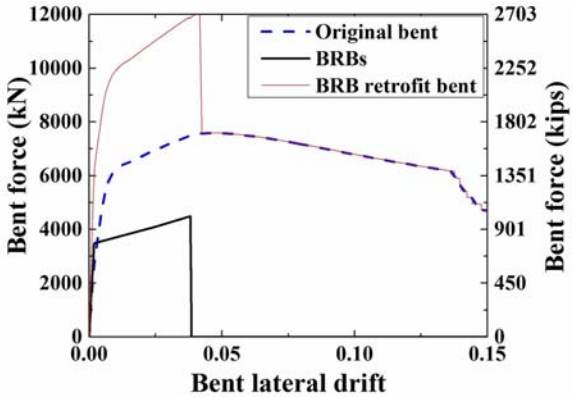

Figure 7. Full scale pushover curves considering collapse capacity of bent and BRBs.

5. INCREMENTAL DYNAMIC ANALYSES OF 3D SKEWED BRIDGES WITH BRBS

The straight bridge used in previous sections is further modified to have different skew abutment angles, α, with respect to the longitudinal axis (Figure 1). The skew angles considered in this study are α = 0° (straight), 18°, 36°, and 54°. Table 2 presents the bridge's first three fundamental periods of vibration

for the original and DS-50BRB retrofit bridge models under different skew angles. Due to the orthogonality of the longitudinal and transverse directions of straight bridge models, the BRB retrofit has negligible influence on the longitudinal frequency. As the skew angle (α) varies from 0° to 54°, the longitudinal period of the original bridge varies by only 3% due to α variations, whereas the skew direction period varies as much as 15%. These variation increases to 25% for the retrofitted bridges due to the stiffness contribution from the BRB components.

Table 2. Bridge periods of vibration.

Bridge Model	1st (Long. Dir.)	2nd (Skew Dir.)	3rd (Vertical Dir.)
α= 0° (Straight), original	0.66	0.38	0.29
α = 18°, original	0.66	0.39	0.29
α = 36°, original	0.65	0.40	0.30
α = 54°, original	0.68	0.44	0.33
α = 0°, DS-50BRB	0.66	0.28	0.29
α = 18°, DS-50BRB	0.64	0.31	0.29
α = 36°, DS-50BRB	0.58	0.32	0.29
α = 54°, DS-50BRB	0.59	0.35	0.33

Note: BRB lateral resistance contribution is 50% (DS-50BRB).

5.1 IDAs of Bridges with Different Skew Angles

The IDA curves in Figure 8 represent the variation of the maximum drift ratio demand as a function of seismic level, S_{a_SRSS} (i.e., S_a/g-θ_{max} relationships). In each time history analysis for the IDAs, two horizontal records are applied in the transverse and longitudinal direction of bridges, which was proved to capture the maximum responses (Wang et al. 2017), as well as one original vertical record. The figure presents individual, median, 16th and 84th percentile IDA curves until structural instability or complete collapse was reached, as evidenced by the plateau in the curves. Compared to straight bridges (Figure 8a), collapse occurs at smaller drift ratios for the bridges with large skew angles (Figure 8b, 8c, and 8d). For example, the median IDA curve of the 54° skewed bridges becomes flat at 10% drift (Figure 8d), while the median IDA of the straight bridge becomes flat at 14% drift (Figure 8a). A large skew angle reduces the record-to-record (RTR) variability since the dispersion of individual responses is reduced by 10% in the 54° skewed bridge model. However, all bridges with different skew angles have a median collapse capacity variation of less than 5%, because the element's section properties are the same.

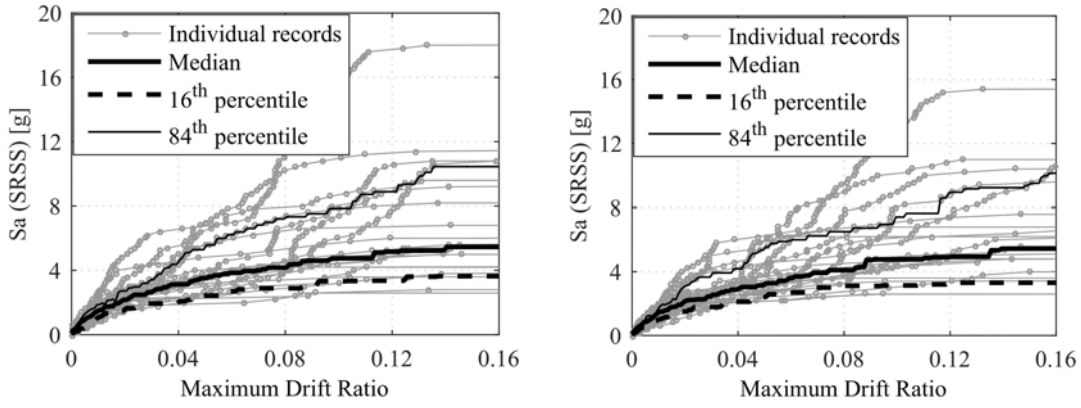

(a) (b)

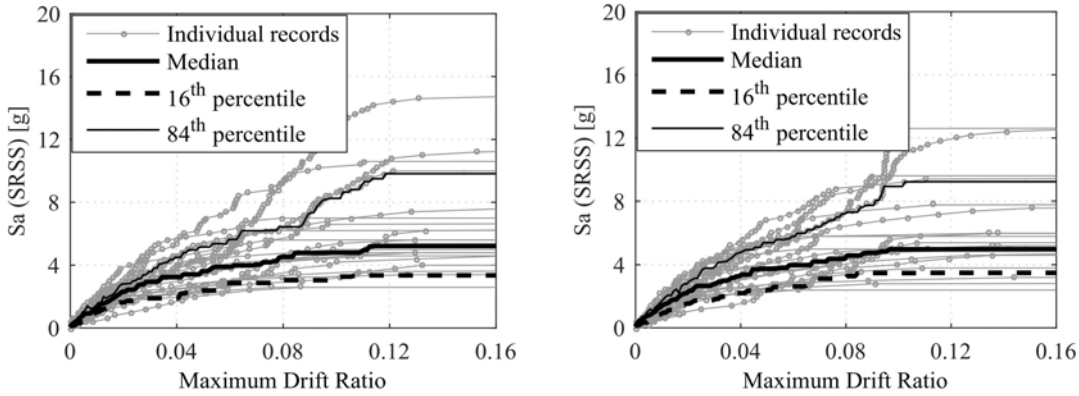

(c) (d)

Figure 8. Sa/g - θmax relationships for bridges with different skew (a) 0°, (b) 18°, (c) 36°, (d) 54°.

5.2 Effects of BRB Retrofit on Incremental Dynamic Analyses

This section evaluates the effect of BRB retrofit on the seismic performance of skewed bridges. The BRBs are assumed to reach complete failure when the BRB core axial strain reaches 3.5%. Figures 9a and 8b show the individual and statistical IDAs for the original and retrofitted bridges with a 36° skew angle, respectively. As observed, the variability is smaller for the bridge with BRBs. For example, at a 12% drift, the BRB components reduce the dispersion due to the RTR variability by 23%.

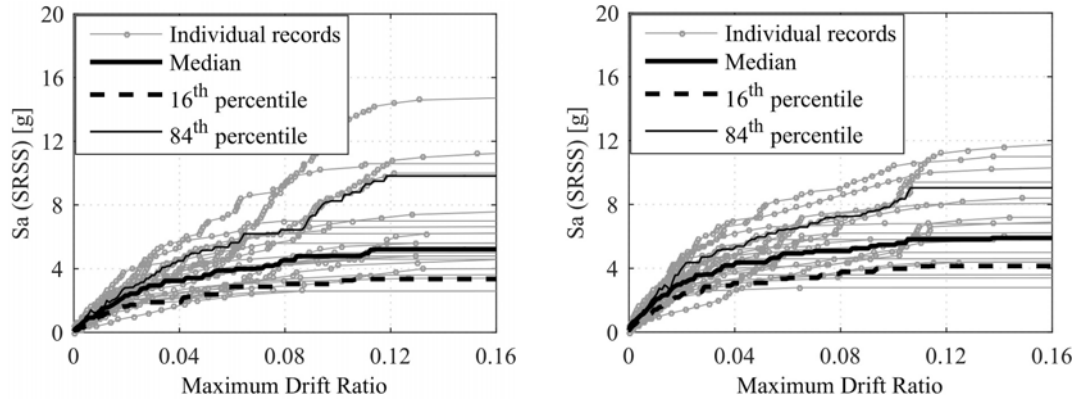

(a) (b)

Figure 9. Sa/g – θmax relationships for 36° skewed bridges (a) Original, (b) Retrofit.

5.3 Mean Annual Frequency of Collapse

To estimate the effect of BRB implementation on the seismic performance of skewed bridges, the mean annual frequency (MAF) of collapse is computed in this section for the original and retrofitted bridges. The MAF of collapse is obtained from numerical integration methods (Jalayer and Cornell 2003, Ibarra and Krawinkler 2005) that combine fragility curves (FCs) obtained from the IDAs, and hazard curves (HCs) obtained for the bridge location (i.e., Ripon, CA). In this study, FCs were calculated in such a way that the drift fragility is distributed along the horizontal direction of the IDA curves. The MAF of collapse was obtained based on a drift limit commonly associated to imminent collapse to encompass the bridge performance at different seismic levels. In this section, the fragility function is derived based on "horizontal statistics" of the maximum bent drifts at different $S_{a_{SRSS}}$(s) (Figure 10). The collapse FC ($F_{C,a_{SRSS},C}$) is obtained from the cumulative probability that the drift is more than or equal to a predefined imminent collapse drift [i.e., 2.5% in this study (OES 1995)] at monotonically increasing seismic levels (i.e., $S_{a_{SRSS}}$), as shown in Equation 4.

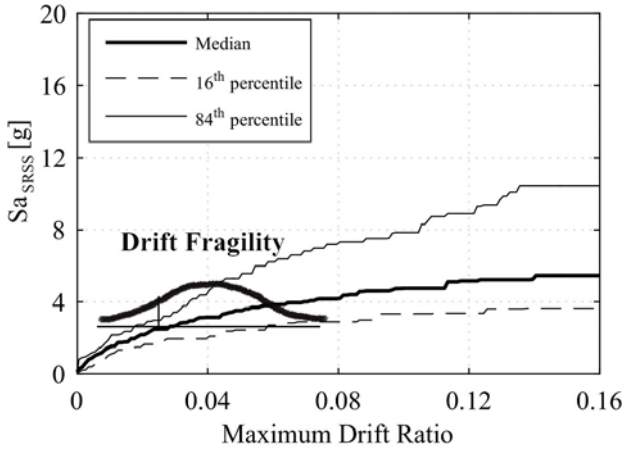

Figure 10. Drift fragility and spectral acceleration fragility.

$$F_{C,a_{SRSS}}(x) = P[D \le d_c | S_{a\_SRSS}/g = x] \quad (4)$$

$$\lambda_c = \int_0^{\infty} FC\,(F_{C,a_{SRSS},c}) \cdot d|\lambda_a(x)| \quad (5)$$

The computed FCs for the 36° skewed bridges before and after being retrofitted with BRBs are shown in Figure 11, assuming an imminent collapse limit state of 2.5% drift ratio. To generate these FCs, the bridges were subjected to 3D ground motion sets, with two scaled horizontal accelerations, and the corresponding original vertical acceleration. The MAF–Orig. and MAF–Retrof. curves in Figure 11 denote the MAF of imminent collapse under monotonically increasing spectral accelerations for the original and retrofitted bridges, respectively. The HC used in the calculations is also shown, as well as the probability distribution functions (PDFs) resulting from the integration in Equation 5. The MAFs of imminent collapse for the original and retrofitted bridges are denoted as λ_{C_Orig} and λ_{C_Retrof}, respectively. In the 36° skewed bridge model, BRB retrofit can reduce the MAF of the imminent collapse from about 6.89×10^{-6} to 1.21×10^{-6}, as shown in Figure 11, with a reduction of approximately 80%. The PDF curves also show that the S_a threshold for potential collapse increases from 0.48 g in the original bridge to approximately 0.80 g in the retrofitted bridge.

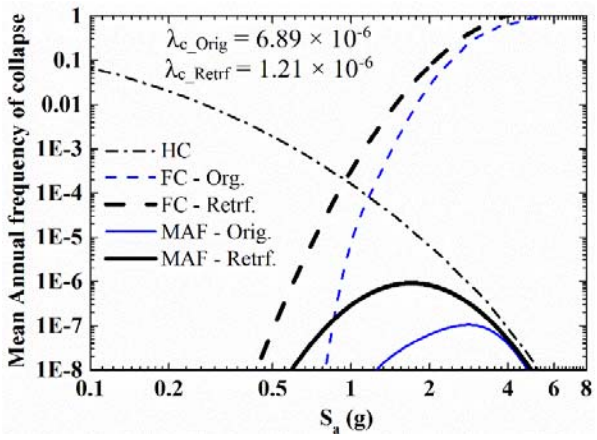

Figure 11. HC, FC, and MAF of the collapse of a 36° skewed bridge due to $S_{a\_SRSS} = x$ at T = 0.5s.

6. CONCLUSIONS

This study provides a systematic approach to estimate the deterioration and collapse capacity of skewed bridges retrofitted with buckling restrained braces (BRBs) by performing three-dimensional incremental dynamic analysis (IDAs), based on a distributed plasticity fiber model. This model was calibrated with a concentrated plasticity model to ensure that it can predict structural instability. The main findings are as follows:

(1) The structural deterioration of the reinforced concrete bridge is caused by concrete crushing, and buckling of the reinforcement, among other factors. The distributed plasticity fiber model can reproduce the material deterioration of concrete bridges and, in combination with predefined BRB failure modes, can predict the seismic behavior and collapse capacity of skewed bridges retrofitted with BRBs.

(2) A larger bridge skew angle has a negligible effect on the median of the maximum lateral drift ratio. However, a larger skew angle reduces record-to-record (RTR) variability by about 10%. This reduction is from the contribution of both horizontal ground motions, and the lack of orthogonality between the longitudinal and the bent direction in skew bridges.

(3) The BRB failure was assumed to be controlled by the air gap length between the concrete and steel core. Typical manufacturer air-gap dimensions lead to a BRB failure limit at about 3.5% axial strain, which is equivalent to a 3.8% bent lateral drift ratio in this study. A second criterion based on BRB cumulative plastic ductility failure indicates that the above failure threshold is an upper limit for the evaluated retrofitted bridge subjected to the 21 FEMA ground motions.

(4) The retrofit increases the bridge collapse capacity at large drifts by only 10 – 15%, since BRBs are assumed to fail at a 3.8% lateral drift ratio. However, the retrofit reduces the bridge mean annual frequency for imminent collapse by 80%, which is defined at a lateral bent drift ratio of 2.5%.

(5) The distributed plasticity model is an effective tool for performing three-dimensional IDAs up to the collapse limit state, as long as adequate constitutive relationships are provided for the concrete and steel materials.

7. ACKNOWLEDGMENTS

The authors are grateful to Mountain Plains Consortium (MPC) for the financial support for this research under project MPC-421. The authors also thank Dr. Peyman Kaviani, Prof. Farzin Zareian and Marta De Bortoli for providing the original bridge model in OpenSees.

8. REFERENCES

Andrews B, Fahnestock L, Song J (2009). Ductility capacity models for buckling-restrained braces. *Journal of Construction Steel Research*, 65(8), 1712-1720.

ASCE. (2007). Seismic rehabilitation of existing buildings (ASCE41-06), Reston, VA.

Bazaez R, Dusicka P (2016). Cyclic behavior of reinforced concrete bridge bent retrofitted with buckling restrained braces. *Engineering Structures*, 119, 34-48.

Billah A, Alam M (2014). Seismic performance evaluation of multi-column bridge bents retrofitted with different alternatives using incremental dynamic analysis. *Engineering Structures*, 62, 105-117.

Caltrans. (1999). Caltrans seismic design criteria version 1.1. Sacramento, CA.

Celik O, Bruneau M (2009). Seismic behavior of bidirectional resistant ductile end diaphragms with buckling restrained braces in straight steel bridges. *Engineering Structures*, 31(2), 380–393.

Dhakal R, Maekawa K (2002). Modeling for post-yield buckled of reinforcement. *ASCE Journal of Structural Engineering*, 128(9): 1139-1147.

El-Bahey S, Bruneau M. (2011). Buckling restrained braces as structural fuses for the seismic retrofit of reinforced concrete bridge bents. *Engineering Structures*, 33(3), 1052–1061.

FEMA. (2009). Quantification of building seismic performance factors, Washington, DC.

Haselton C, Deierlein G (2007). Assessing seismic collapse safety of modern reinforced concrete moment frame buildings. Pacific Earthquake Engineering Research Center, Berkeley, CA.

He R, Yang Y, Sneed L (2016). Post-repair seismic assessment of RC bridges damaged with fractured column bars – A numerical approach. *Engineering Structures*, 112, 100-113.

Ibarra L, Krawinkler H (2005). Global collapse of frame structures under seismic excitations. Pacific Earthquake Engineering Research Center, Berkeley, CA.

Jalayer F, Cornell C (2003). A technical framework for probability-based demand and capacity factor (DCFD) seismic formats. Earthquake Engineering Research Center, Berkeley, CA.

Kaviani P, Zareian F, Taciroglu E (2012). Seismic behavior of reinforced concrete bridges with skew-angled seat-type abutments. *Engineering Structures*, 45, 137-150.

Lignos D, Krawinkler H, Whittaker A. Prediction and validation of sidesway collapse of two scale models of a 4-story steel moment frame. *Earthquake Engineering & Struct Dynamic 2011*; 40 (7): 807-825.

Lowes L, Moehle J (1995). Seismic behavior and retrofit of older reinforced concrete bridge T-Joints. *Rep. No. UCB/EERC-95/09*, Grand Forks, ND.

Mander J, Priestley M, Park R (1988). Observed stress-strain behavior of confined concrete. *ASCE Journal of Structure Engineering,* 114(8), 1827-1849.

Marsh A (2013). Evaluation of passive force on skewed bridge abutments with large-scale tests. *Ph.D. Dissertation*, Brigham Young University, Provo, UT.

Mazzoni S, Moehle J, Mahin S (1997). Design and response of lower-level beam-column joints in ductile reinforced concrete double-deck bridge structures. Earthquake Engineering Research Center, Berkeley, CA.

McKenna F (2010). Open system for earthquake engineering simulation. University of California, Berkeley.

OES (Office of Emergency Services). Vision 2000 (1995). Performance based seismic engineering of buildings, Structural Engineers Association of California, Sacramento, CA.

Pantelides C, Ibarra L, Wang Y, Upadhyay A (2016). Seismic rehabilitation of skewed and curved bridges using a new generation of buckling restrained braces. *Rep. No. MPC 16-315.*, Fargo, ND.

Rollins K, Jessee S (2012). Passive force-deflection curves for skewed abutments. *Journal of Bridge Engineering*, 18(10), 1086-1094.

Scott B, Park R, Priestley M. (1982). Stress-strain behavior of concrete confined by overlapping hoops at low and high strain rates. *Journal of ACI*, 79, 13-27.

Upadhyay A, Pantelides C (2017). Comparison of the seismic retrofit of a three-column bridge bent with buckling restrained braces and self centering braces. *Proceeding of the Structures Congress 2017*, Denver, CO.

Vamvatsikos D, Cornell CA (2002). Incremental dynamic analysis. *Earthquake Engineering & Structural Dynamics*, 31(3): 491-514.

Vamvatsikos D, Sigalas I (2005). Seismic performance evaluation of a horizontally curved highway bridge using incremental dynamic analysis in 3D. *Proceedings of the 4th European workshop on Seismic Behavior of Irregular and Complex Structures*, Thessaloniki, Greece.

Wang Y, Ibarra L, Pantelides C (2016). Seismic retrofit of a three-span RC bridge with buckling-restrained braces. *Journal of Bridge Engineering*, 21(11): 04016073.

Wang Y, Ibarra L, Pantelides C (2017). Effects of Ground Motion Incidence Angles in a Reinforced Concrete Skewed Bridge Retrofitted with Buckling Restrained Braces. *Proceedings of the Structures Congress 2017, Denver, CO.*

Xu W, Pantelides C (2017). Strong-axis and weak-axis buckling and local bulging of buckling-restrained braces with prismatic core plates. *Engineering Structures*, 153, 279-289.